ACS OMEGA

http://pubs.acs.org/journal/acsodf

Article

Structural Effect of Polyimide Precursors on Highly Thermally Conductive Graphite Films

Jeong-Un Jin, Jae Ryang Hahn, and Nam-Ho You*

Cite This: *ACS Omega* 2022, 7, 25565−25572

Read Online

ACCESS | Metrics & More | Article Recommendations | Supporting Information

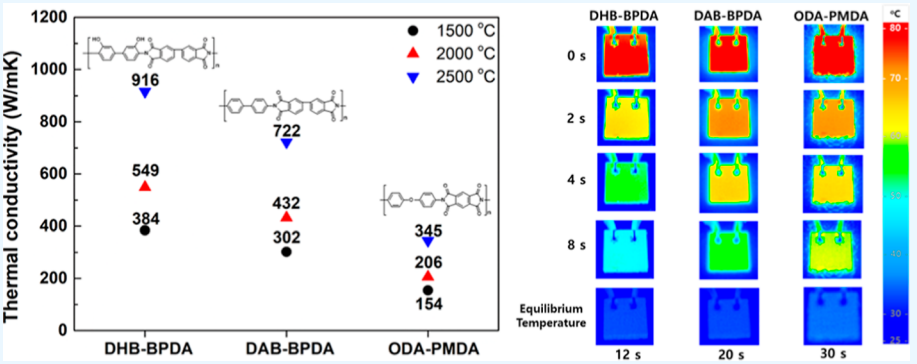

ABSTRACT: In this study, polyimide (PI) with high carbonization yield was used as a precursor to prepare graphite films with high thermal conductivity. The crystallinity, grain size, and thermal conductivity of the graphite films were characterized and found to vary according to the chemical structure of the PI precursor. Aromatic PIs containing ortho-substituted hydroxyl groups in the PI main chain (DHB-BPDA) were synthesized by the polycondensation reaction of 3,3′-dihydroxybenzidine (DHB) and 3,3′,4,4′-biphenyltetracarboxylic dianhydride (BPDA). The DHB-BPDA is converted to a polybenzoxazole (PBO) structure through thermolysis reaction during carbonization. The PBO containing a benzene ring and a heterocycle group can provide a strong main chain and high thermal stability due to its resonant structure. The graphite film prepared from DHB-BPDA exhibited a large grain size (63.727 nm) and a high thermal conductivity of 916 W/(mK).

1. INTRODUCTION

High-powered electronic devices used in smartphones, automobiles, and electric transmission fields are becoming increasingly lightweight, thin, and miniaturized.[1] Since high-power equipment generates more heat due to its high power, miniaturization can degrade the function of the device.[1,2] Therefore, many interesting research studies are being focused on technologies to control the emitted heat. In particular, the demand for high heat dissipation materials that have low density and high thermal conductivity is rapidly increasing.[3] Although metal materials have high thermal and electrical conductivity, their applications are limited as heat dissipation materials because of their high density and brittleness. Polymer materials have many advantages such as good insulation, low density, and low thermal conductivity. Extensive efforts are underway to improve their thermal conductivity while meeting other requirements. Aromatic polyimides (PIs) are one group of engineering plastics extensively used in aerospace, microelectronics, and insulating and fire-resistant materials due to their advantageous properties. They have remarkably high mechanical strength, thermal stability, and chemical and radiation resistance.[4−7] Recently, PIs have attracted much attention as effective carbon precursors because of their unique molecular structure and high carbon yield. Various studies have demonstrated that PIs can be converted into carbon materials using simple carbonization and graphitization procedures.[8−11] There are many ways to improve the heat dissipation performance of graphite films. One is to introduce a hybrid component such as graphene, iron, or silicon carbide into the polymer matrix. A high thermal conductivity material can form a thermally conductive network or conduction path, leading to an improvement in thermal conductivity or the formation of a highly oriented graphite film.[12,13]

However, while the introduction of a highly thermally conductive filler into a PI matrix can help to induce directional growth and high thermal conductivity, it is very difficult to avoid impurities, agglomeration, and non-uniform dispersion. At the same time, some defects can cause small lattice size,

Received: May 2, 2022
Accepted: June 29, 2022
Published: July 12, 2022

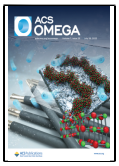

Scheme 1. Synthesis of Polyimides

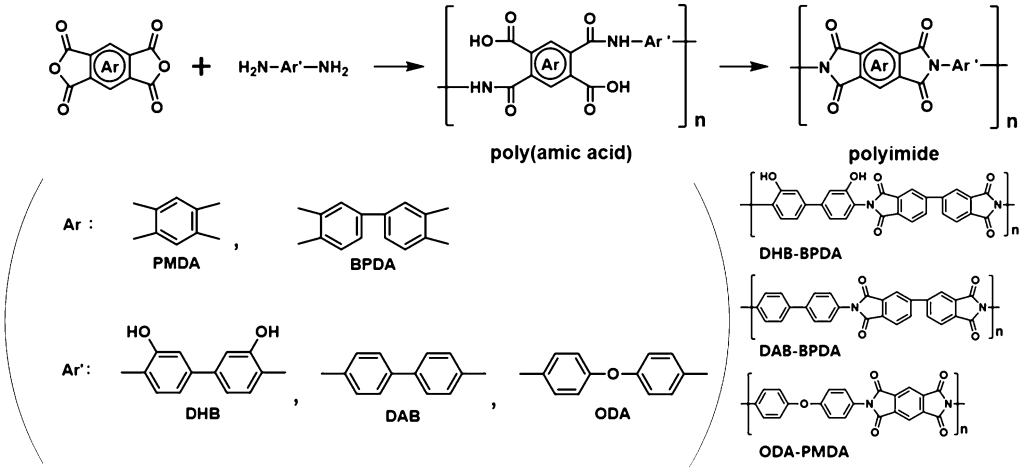

large defects, and disorder between the graphite layers, which can reduce thermal conductivity.[14−17]

Another way to induce orientation and graphitization in a graphite film without additives is by using a controlled graphitization temperature and a PI precursor with a controlled structure.[10,18−20]

In previous research, various attempts have been made to improve the thermal conductivity and other properties of graphite films by using blended or cross-linked polymers as the carbon precursor.[21,22] However, it is still a great challenge to manage thermal conductivity and other desirable properties.

In this study for graphite films, we designed and synthesized aromatic PIs derived from aromatic diamines 3,3′-dihydroxybenzidine (DHB), 4,4′-diaminodiphenyl ether (ODA), and aromatic dianhydrides such as pyromellitic dianhydride (PMDA), 3,3′,4,4′-biphenyltetracarboxylic dianhydride (BPDA) via a simple two-step polycondensation reaction. After the carbonization and graphitization processes, the graphite films exhibited high thermal conductivity without any catalyst or additives. In particular, the graphite film produced by DHB-BPDA showed high crystallinity and thermal conductivity. This is because the ortho-substituted hydroxyl groups in the PI main chain can promote thermal rearrangement from PI to polybenzoxazole (PBO).[23−26] The high thermal stability and strong intermolecular interaction of the PBO were due to the resonance structure between polymer chains, which improved carbon yield, crystallinity, and film retention during the graphite film production. This study provides valuable information about the structural effects of polyimide precursors on highly thermally conductive graphite films.

2. EXPERIMENTAL SECTION

2.1. Materials. 3,3′-Dihydroxybenzidine (DHB), 4,4′-diaminodiphenyl ether (ODA), pyromellitic dianhydride (PMDA), 3,3′,4,4′-biphenyltetracarboxylic dianhydride (BPDA), and 4,4′-dinitrobiphenyl were obtained from Tokyo Chemical Industry Co., Ltd. Hydrazine hydrate (80%, solution in water), 1-methyl-2-pyrrolidinone (NMP, 99.5%, anhydrous), and 10 wt % palladium-loaded matrix-activated carbon support (Pd/C) were obtained from Sigma-Aldrich. All chemicals and reagents were used as received, without purification.

2.2. Preparation of Polyimide Films. Poly (amic acid, PAA) was synthesized from an aromatic diamine, such as DHB and ODA, and an aromatic dianhydride, such as PMDA and BPDA, via a simple two-step polycondensation reaction. The reaction was carried out at room temperature using NMP with an equivalent molar ratio of diamine and dianhydride. In step 1, DHB (2.1456 g, 20 mmol) was added and completely dissolved in NMP (5.9 g, 10 wt % solids in solution) in a 70 mL vial. Then, BPDA (5.884 g, 20 mmol) was added to the solution and magnetically stirred for 24 h to prepare a PAA solution. All PAA precursors were prepared by the same procedure. In step 2, in the thermal imidization process, PAA solution was cast on a glass plate and then treated at 80, 120, 180, 250, and 350 °C in an argon atmosphere for 1 h. Scheme 1 shows the process and chemical structure of PI. The PI films were indicated by DHB-BPDA, DAB-BPDA, and ODA-PMDA. The inherent viscosities of the PAA were 0.83−0.94 dL/g in a concentration of 0.5 g/dL of NMP solution at 30 °C (Table 1).

Table 1. Inherent Viscosity of PAA and Thermal Properties of the PI Films

polyimide	$[\eta]_{inh}$ [a] (dL/g)	$T_{d5\%}$ [b] [°C]	$T_{d10\%}$ [b] [°C]	char yield % (at 800 °C)
DHB-BPDA	0.94	421	444	64
DAB-BPDA	0.85	587	600	67
ODA-PMDA	0.83	540	556	58

[a]Inherent viscosity of PAA measured at a concentration of 0.5 g/dL of NMP solution at 30 °C. [b]$T_{d5\%}$ and $T_{d10\%}$: temperatures at 5 and 10% weight loss, respectively.

2.3. Carbonization and Graphitization of the PI Films. Figure 1 shows the preparation process of the PI film and graphite film. The PI film was inserted between polished artificial graphite plates to prevent dust contamination from the furnace and to minimize deformation. Carbonized films were prepared by maintaining a heating rate of 10 °C/min at 1000 and 1500 °C for 2 h.

Graphitized PI films were prepared by using carbonized PI films at 1000 °C. The graphitization process was maintained for 2 h by heating to 1500 °C at a rate of 10 °C/min and heating to 2000 and 2500 °C at a heating rate of 5 °C/min.

https://doi.org/10.1021/acsomega.2c02731
ACS Omega 2022, 7, 25565−25572

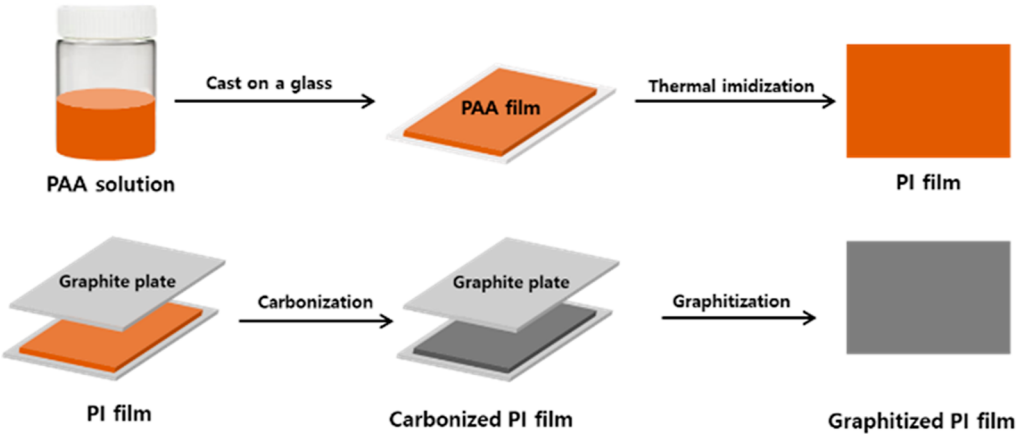

Figure 1. Preparation process for graphitized PI films.

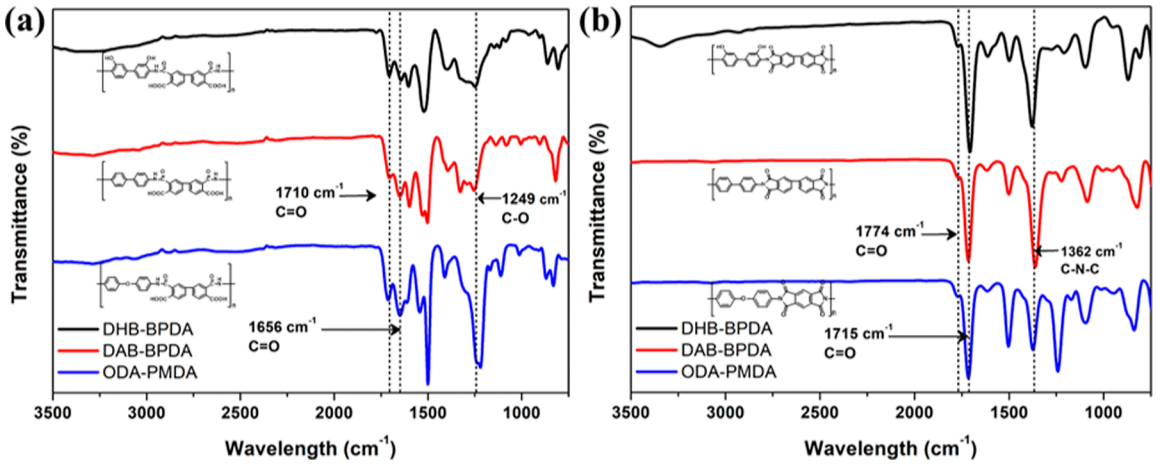

Figure 2. FT-IR spectra of (a) PAA and (b) PI films.

The optical images of the PI films and graphitized films at 2500 °C are shown in Figure S1.

2.4. Characterization. FT-IR spectra of the PAA, PI, and PBO were obtained with 32 sans (2 cm^{-1} resolution) in the ATR mode by FT-IR spectroscopy (Nicolet IS10, USA). X-ray diffraction patterns were obtained on an XRD (SmartLab, Rigaku Corporation, Japan) with (voltage of 40 kV, current of 30 mA) Cu Kα radiation (λ = 0.154 nm). Thermogravimetric analysis (TGA) curves of the PI films were measured up to 800 °C at 10 °C/min in a nitrogen atmosphere using a Q 50 (TA Instruments, USA). Raman spectroscopy of the carbonized and graphitized PI films was performed with a high-resolution Raman spectrometer (LabRAM HR, Horiba Scientific, Japan). The X-ray photoelectron spectroscopy (XPS) spectra were measured using a spectrophotometer (K-alpha, Thermo Fisher Scientific, USA). A standard Al Kα (1486.6 eV) at 14.9 keV anode voltage was used as the excitation source. The filament current was 4.6 A, and the emission current was 20 mA. SEM images of the fractured cross-sections of the graphite films were obtained with scanning electron microscopy (SEM; Nova NanoSEM 650, FEI Company, Netherlands). TEM images of graphite films were obtained by fast Fourier transform with terminal electron microscopy (TEM; FEI Titan Cubed Themis G2 60-300, FEI Company, Netherlands). The graphite film was prepared with a thickness of about 40 μm in a size of 0.5 cm × 3 cm, and the thermal diffusivity was performed with the Laser PIT-M2 (Ulvac-Riko, Japan). Infrared thermal images were observed with a Testo-875i basic (Testo AG, Germany) infrared camera with a ceramic electrode (1 cm × 1 cm) as a heating element and graphite films. A non-destructive 3D image of the inside of the graphite film was obtained using Ultra X-ray. X-ray computed tomography (CT) was performed using a Zeiss Xradia 520 Versa (XCT: Zeiss Xradia 520 Versa X-ray CT, Carl Zeiss, Germany), and the maximum output of X-rays was 10 W. The measured results were a reconstruction of object research software (ORS) by Carl Zeiss.

3. RESULTS AND DISCUSSION

3.1. Characterizations of PI Films. Figure 2 shows the FT-IR spectra of the (Figure 2a) PAA and (Figure 2b) PI films. Figure 2a shows 1249 cm^{-1} (C−O str.), 1548 cm^{-1} (N−H str.), and 1656 and 1710 cm^{-1} (C═O str.) peaks. After thermal curing, the PI spectra were 1362 cm^{-1} (C−N−C, str.), 1500 cm^{-1} (C═C str.), 1715 cm^{-1} (sym, C═O str.), and 1774 cm^{-1} (asym. C═O str.). Changes in these peaks clearly indicated complete conversion to PI. The FT-IR spectra of PAA, PI, and PBO prepared from DHB-BPDA are shown in Figure S2, and absorption at 1612 and 1076 cm^{-1} represents the formation of benzoxazole rings, and thermal conversion from PI to PBO was confirmed.[23,27]

The TGA curves of the PI film are shown in Figure 3. The PI film showed a weight loss temperature of 5% in the range of 420−590 °C. The $T_{d5\%}$ temperature of the DHB-BPDA was 421 °C, with weight loss originating from the thermal

https://doi.org/10.1021/acsomega.2c02731
ACS Omega 2022, 7, 25565−25572

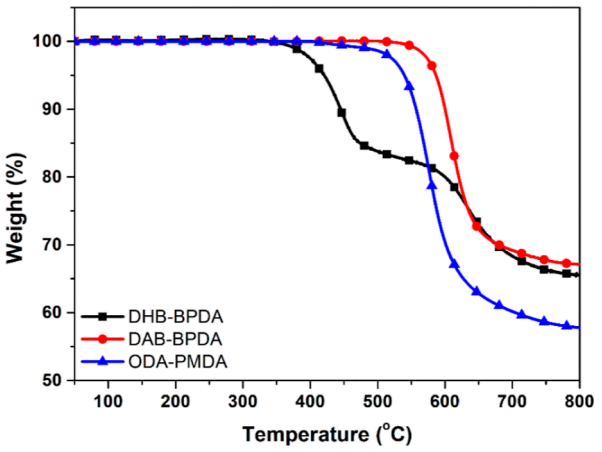

Figure 3. TGA curves of PI films (at a heating rate of 10 °C/min with N_2 gas).

conversion of PI to PBO. In the thermal conversion process, the hydroxyl group attacks the carbonyl group to form an oxazole ring, and water is released as a by-product.[23,25] The TGA curves according to PAA, PI, and PBO thermal conversion of the DHB-BPDA structure are shown in Figure S3. The char yield of PBO was the highest residual amount, about 73%, and the char yield of all PI films was over 55% at 800 °C.

Optical images of the PI films and graphitized PI films at 2500 °C are shown in Figure S1. Reddish-brown and yellow PI films were finally prepared for silver-white, silver-dark gray, and dark-colored graphite films through carbonization and graphitization. These differences are associated with the various carbon structures formed according to the chemical structure of the precursor.[28−30]

3.2. Characterizations of Graphite Films. Figure 4 shows the XRD patterns of the carbonized and graphitized PI films at various temperatures. The pattern of the PI film in Figure 4a shows a diffraction peak in the crystal field and a dispersion peak in the amorphous region. This pattern suggests that the PI has a semi-crystalline phase.[28,29] For example, the DAB-BPDA PI exhibits two strong reflections at 14 and 24°. The DHB-BPDA PI showed peaks at 14, 22, and 26°; ODA-PMDA showed a broad reflection peak at 18°. BPDA showed high crystallinity, and DHB, including hydroxyl groups, showed relatively lower crystallinity than the DAB. The XRD pattern results of the PI films were characterized differently due to differences in molecular chains.

In Figure 4a−c, all of the carbonized PI films exhibit relatively broad carbon peaks near 25° of the carbon (002) peak. Here, the broad peaks suggest that there is a lot of low crystallinity and amorphous carbon. As the temperature increases, the peak (002) becomes larger and sharper as it moves to about 26°. This proves that grain sizes grew during the carbon conversion process, and the films formed a regular graphite structure. In addition, the sharpest peak appeared in the graphitized DHB-BPDA structure at 2500 °C.

It has been demonstrated that the chemical structure of PI films affects the degree of graphitization. The interlayer distance and grain size of the graphitized film at 2500 °C were calculated according to the Scherer eqs 1 and 2.[30,31]

$$\lambda = 2d_{002}\sin\theta \quad (1)$$

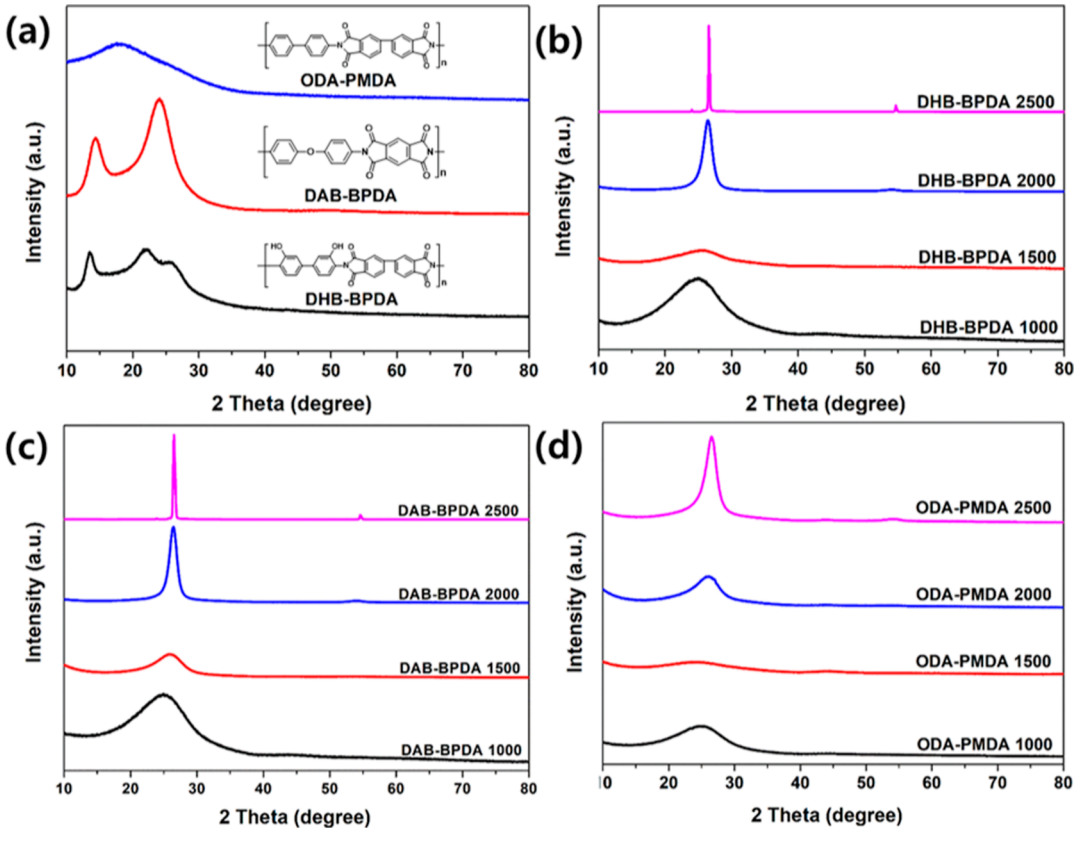

Figure 4. (a) XRD patterns of PI films, carbonized and graphitized PI films, (b) DHB-BPDA, (c) DAB-BPDA, and (d) ODA-PMDA.

https://doi.org/10.1021/acsomega.2c02731
ACS Omega 2022, 7, 25565−25572

$$D = \frac{0.89\lambda}{\mathrm{B}\ \cos\theta} \quad (2)$$

The calculated grain parameters are shown in Table 2. The interlayer distance of the graphite films had similar values, but

Table 2. Related Parameters of XRD Results[a]

samples	2θ (°)	FWHM	d_{002} (nm)	D (nm)
DHB-BPDA	26.545	0.221	0.335	63.727
DAB-BPDA	26.532	0.338	0.336	41.667
ODA-PMDA	26.439	1.05	0.337	13.410

[a]All samples of PI films graphitized at 2500 °C.

the grain size was different due to the significant difference in full width at half maximum. This difference proves that crystallinity and grain size are affected by the PI precursor structure. The grain size of DHB-BPDA was 63.727 nm, which was larger than that of the other samples.[32]

The Raman spectra of the carbonized and graphitized PI films are shown in Figure 5. Two peaks are identified at 1300 cm^{-1} (D-band) and 1580 cm^{-1} (G-band), and the ratio of the signal intensity indicates the carbon material's defects. The carbonized PI films at 1000 °C showed both D and G peaks, indicating the existence of a disordered carbon structure and amorphous carbon. As the temperature increases, the defect decreases significantly, and 2D peaks occur. The I_D/I_G ratio decreases sharply above 2000 °C, and a 2D peak appears. The 2D peak means that a multi-layer structure was formed during the graphitization process. The D peak of the PI film graphitized at 2500 °C is hardly seen, suggesting that a high-quality graphite film was prepared. DHB-BPDA, which showed high crystallinity and large grain size in XRD, confirmed that the I_D/I_G ratio was zero. The I_D/I_G ratio tended to decrease as the crystallinity of the graphite film increased.

XPS spectroscopy was performed with the PI film graphitized at 2500 °C. The C1s spectrum in Figure 6 consisted of three peaks at about 285.08, 286.0, and 287.4 eV, indicating C═C/C−C, C−OR, and C−O−C bonds, respectively. The ratio of the three peaks was different depending on the structure of the PI precursor, which is related to the various carbon structures formed according to the chemical structure of the precursor. The DHB-BPDA with high crystallinity and a large grain size had a relatively large C═C/C−C bond ratio.

Figure 7 shows SEM images of cross-sections of the PI films graphitized at 2500 °C. The graphite film was aligned and had a strong orientation in the plane. The cross-section in Figure 7c has a layered structure, but Figure 7a,b shows smooth and highly oriented cross-sections. In addition, all films appeared without pores or defects caused by carbon, oxygen, nitrogen, and hydrogen, which are generated by the thermal decomposition of functional groups. The chain rearrangement and graphite multi-layer growth gradually progressed during the graphitization process, using PI film carbonized at 1000 °C. The inner pores and other defects of the graphite film were effectively removed using a low heating rate.[8,33]

Figure S5a−c display images from inside the PI films graphitized at 2500 °C by 3D X-ray CT tomography. The inside of the graphite film was monitored at a resolution of 100 nm. The 3D image converted through ORS was displayed at a size of 40 × 7 × 40 μm^3, and a clean interior without pores or defects was confirmed.

Figure 8 shows the TEM image of the graphitized films at 2500 °C. TEM images show distinct directional layer structures and dense multilayers, which are advantageous in graphite films for in-plane heat transfer. The interlayer spacing of the DAB-BPDA graphene layer was 0.337 to 0.339 nm (XRD 0.336 nm), while the DHB-BPDA was 0.336 nm (XRD 0.335). All errors between the XRD calculation results were less than 2.1%, caused by other test methods, and were within acceptable limits. The results showed that DHB-BPDA was more advantageous for preparing graphite films. The SEAD image showed that DHB-BPDA had better crystallinity than ODA-PMDA. The high crystallinity observed by XRD and the results showing low Raman defects were also consistent with this observation. Overall, it was proved that the DHB-BPDA graphite film provided an excellent foundation for high thermal conductivity.[34]

The thermal conductivity of the carbonized and graphitized PI films is shown in Figure 9. The thermal conductivity of the PI films graphitized at 2500 °C exceeded 340 W/mK. The thermal conductivity according to the PI precursor was confirmed to be of similar levels of crystallinity and grain size depending on the temperature, and the Raman defect result was consistent. In particular, DHB-BPDA exhibited excellent thermal conductivity and significantly exceeded that of all other samples, as shown in Table 3.

The measuring device used to compare the heat dissipation function is shown in Figure 10a. A ceramic electrode was used as the heating device, and it reached a maximum temperature

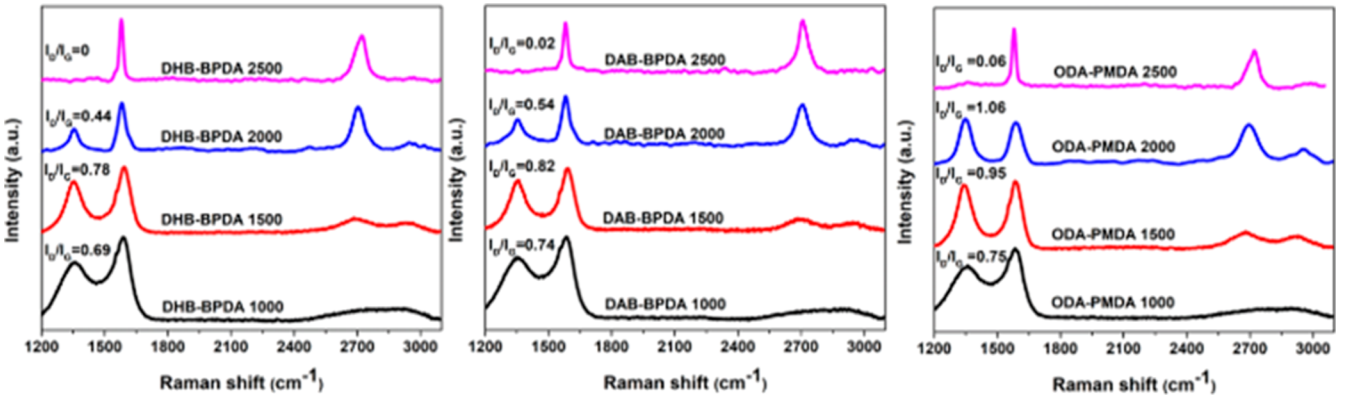

Figure 5. Raman spectra of carbonized and graphitized PI films.

https://doi.org/10.1021/acsomega.2c02731
ACS Omega 2022, 7, 25565−25572

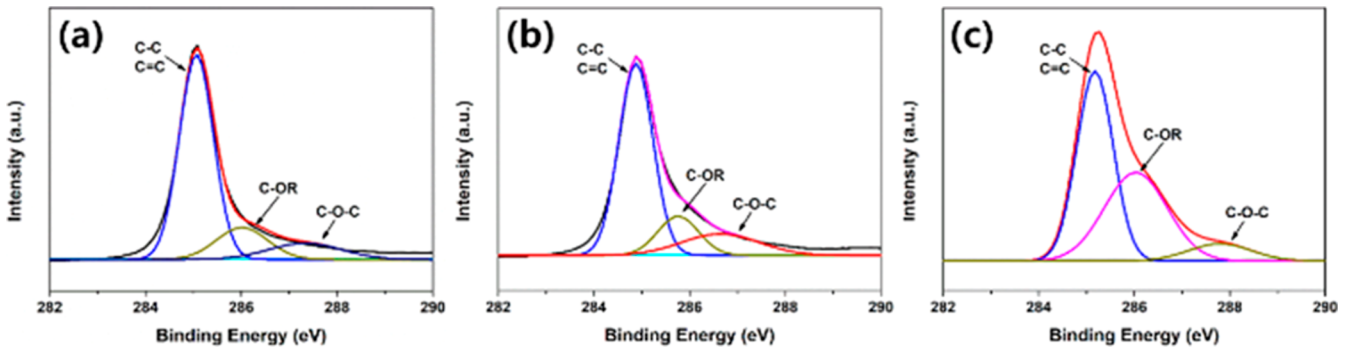

Figure 6. XPS spectrum of PI films graphitized at 2500 °C. (a) DHB-BPDA, (b) DAB-BPDA, and (c) ODA-PMDA.

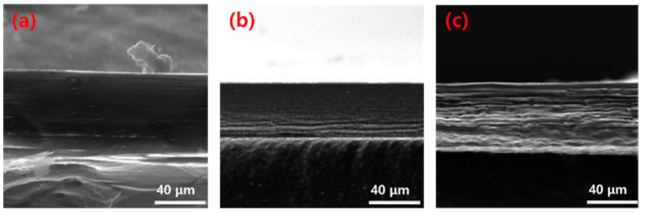

Figure 7. SEM photographs of the cross-section of PI films graphitized at 2500 °C. (a) DHB-BPDA, (b) DAB-BPDA, and (c) ODA-PMDA.

of 80 °C at a constant voltage of 5 V. Infrared thermal images in Figure 10b showed that the heat from the ceramic electrode rapidly decreased and diffused into the graphite film. When used as a heat sink in DHB-BPDA, which had the highest thermal conductivity, the temperature rapidly decreased and stabilized. DHB-BPDA has great potential in the field of in-plane thermal conductivity. Using XRD, Raman, XPS, and TEM analysis, the results of the crystallinity, grain size, and multilayered interlayer distance were consistent.

4. CONCLUSIONS

PI precursors were designed and synthesized to produce graphite films with high thermal conductivity. The PI films were prepared by the thermal imidization of PAA. All of the graphite films prepared at 2500 °C showed thermal conductivity in the range of 345−916 W/mK. In particular, the graphite film derived from PI containing ortho-substituted hydroxyl groups in the PI main chain (DHB-BPDA) exhibited excellent characteristics. This is because DHB-BPDA is converted to a polybenzoxazole (PBO) structure through the thermolysis reaction during carbonization, which results in a

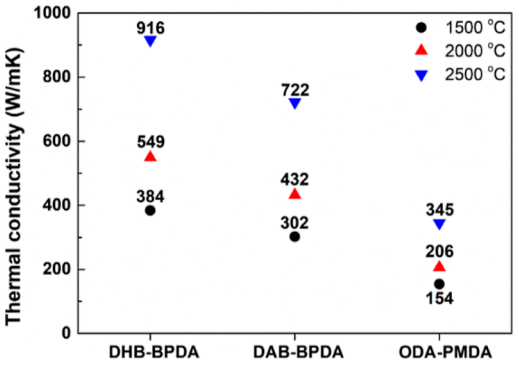

Figure 9. Thermal conductivity of in-plane carbonized and graphitized PI films.

Table 3. Thermal Conductivity of Graphitized Pure PI in the Literature[a]

refs	method	graphitization temperature (°C)	thermal conductivity (W/mK)
12	pure PI film (ODA-PMDA)	2500	332.9
33	pure PI film (ODA-PMDA)	2950	22.2
35	pure PI fiber (ODA-PMDA)	2800	256
36	pure PI foam (ODA-PMDA)	3000	296.6
this work	pure PI film (DHB-BPDA)	2500	916

[a]All samples were prepared by different procedures.

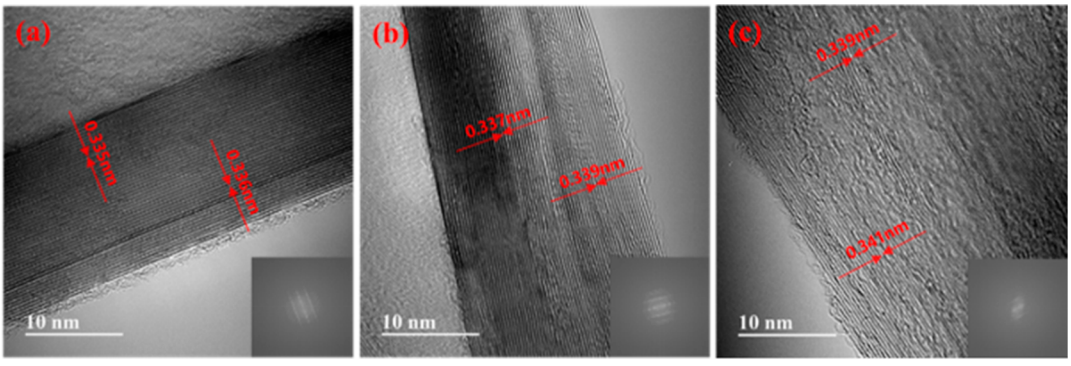

Figure 8. TEM images of PI films graphitized at 2500 °C. (a) DHB-BPDA, (b) DAB-BPDA, and (c) ODA-PMDA.

https://doi.org/10.1021/acsomega.2c02731
ACS Omega 2022, 7, 25565−25572

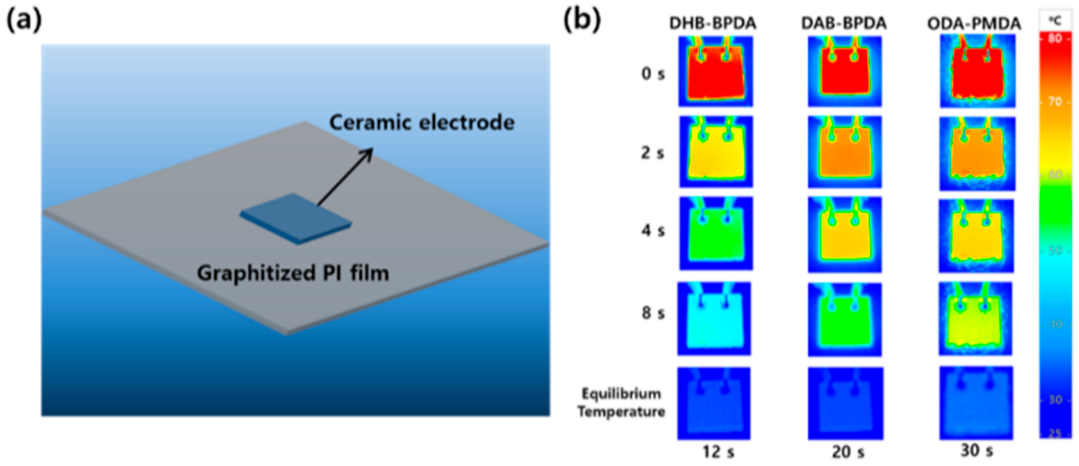

Figure 10. (a) Schematic diagram of a measuring device for heat dissipation capability and (b) infrared thermal images of the ceramic electrode placed on PI films graphitized at 2500 °C.

graphite film with high crystallinity and a large grain size. These highly thermally conductive graphite films indicate that PIs are promising candidates for advanced device applications.

■ ASSOCIATED CONTENT

Supporting Information

The Supporting Information is available free of charge at https://pubs.acs.org/doi/10.1021/acsomega.2c02731.

Experimental details, optical images of films, FT-IR spectra, TGA curves, elemental analysis, density of graphitized PI films, and 3D X-ray tomography images (PDF)

■ AUTHOR INFORMATION

Corresponding Author

Nam-Ho You − *Institute of Advanced Composite Materials, Korea Institute of Science and Technology (KIST), Jeonbuk 55324, Republic of Korea;* orcid.org/0000-0001-8886-226X; Email: polymer@kist.re.kr

Authors

Jeong-Un Jin − *Institute of Advanced Composite Materials, Korea Institute of Science and Technology (KIST), Jeonbuk 55324, Republic of Korea; Department of Chemistry and Research Institute of Physics and Chemistry, Jeonbuk National University, Jeonju 54896, Republic of Korea*

Jae Ryang Hahn − *Department of Chemistry and Research Institute of Physics and Chemistry, Jeonbuk National University, Jeonju 54896, Republic of Korea*

Complete contact information is available at: https://pubs.acs.org/10.1021/acsomega.2c02731

Notes

The authors declare no competing financial interest.

■ ACKNOWLEDGMENTS

The work was partly supported by a grant from the Korea Institute of Science and Technology Institutional (KIST) Program, and this research was also supported by the Korea Evaluation Institute of Industrial Technology (KEIT) and the Ministry of Trade, Industry & Energy (MOTIE) of the Republic of Korea (nos 20011577 & 20011153).

■ REFERENCES

(1) Zhang, F.; Feng, Y.; Feng, W. Three-dimensional interconnected networks for thermally conductive polymer composites: design, preparation, properties, and mechanisms. *Mater. Sci. Eng., R* **2020**, *142*, 100580.

(2) Li, Y.; Zhu, Y.; Jiang, G.; Cano, Z. P.; Yang, J.; Wang, J.; Liu, J.; Chen, X.; Chen, Z. Boosting the Heat Dissipation Performance of Graphene/Polyimide Flexible Carbon Film via Enhanced Through-Plane Conductivity of 3D Hybridized Structure. *Small* **2020**, *16*, 1903315.

(3) Huang, X.; Zhi, C.; Lin, Y.; Bao, H.; Wu, G.; Jiang, P.; Mai, Y.-W. Thermal conductivity of graphene-based polymer nanocomposites. *Mater. Sci. Eng., R* **2020**, *142*, 100577.

(4) Moore, A. L.; Shi, L. Emerging challenges and materials for thermal management of electronics. *Mater. Today* **2014**, *17*, 163−174.

(5) Inagaki, M.; Hishiyama, Y.; Kaburagi, Y. Effect of heating rate during carbonization on graphitization of carbon films derived from aromatic polyimides. *Carbon* **1994**, *32*, 637−639.

(6) Inagaki, M.; Hishiyama, Y. Structural and textural changes from polyimide Kapton to graphite: Part II. Magnetoresistance and x-ray diffraction. *J. Mater. Res.* **1992**, *7*, 1174−1177.

(7) Hishiyama, Y.; Yoshida, A.; Kaburagi, Y.; Inagaki, M. Graphite films prepared from carbonized polyimide films. *Carbon* **1992**, *30*, 333−337.

(8) Hishiyama, Y.; Nakamura, M.; Nagata, Y.; Inagaki, M. Graphitization behavior of carbon film prepared from high modulus polyimide film: synthesis of high-quality graphite film. *Carbon* **1994**, *32*, 645−650.

(9) Ma, L.; Wang, Y.; Xu, X.; Wang, Y.; Wang, C. Structural evolution and thermal conductivity of flexible graphite films prepared by carboxylic graphene/polyimide. *Ceram. Int.* **2021**, *47*, 1076−1085.

(10) Li, J.; Zhang, P.; He, H.; Shi, B. Enhanced the thermal conductivity of flexible copper foil by introducing graphene. *Mater. Des.* **2020**, *187*, 108373.

(11) Potts, J. R.; Dreyer, D. R.; Bielawski, C. W.; Ruoff, R. S. Graphene-based polymer nanocomposites. *Polymer* **2011**, *52*, 5−25.

(12) Paul, D. R.; Robeson, L. M. Polymer nanotechnology: nanocomposites. *Polymer* **2008**, *49*, 3187−3204.

(13) Hatori, H.; Yamada, Y.; Shiraishi, M. In-plane orientation and graphitizability of polyimide films: II. Film thickness dependence. *Carbon* **1993**, *31*, 1307−1312.

(14) Bourgerette, C.; Oberlin, A.; Inagaki, M. Structural and textural changes from polyimide Kapton to graphite: Part I. Optical microscopy and transmission electron microscopy. *J. Mater. Res.* **1992**, *7*, 1158−1173.

(15) Takeichi, T.; Eguchi, Y.; Kaburagi, Y.; Hishiyama, Y.; Inagaki, M. Carbonization and graphitization of BPDA/PDA polyimide films: effect of structure of polyimide precursor. *Carbon* **1999**, *37*, 569−575.
(16) Inagaki, M.; Tachikawa, H.; Nakahashi, T.; Konno, H.; Hishiyama, Y. The chemical bonding state of nitrogen in kapton-derived carbon film and its effect on the graphitization process. *Carbon* **1998**, *36*, 1021−1025.
(17) Inagaki, M.; Meng, L.-J.; Ibuki, T.; Sakai, M.; Hishiyama, Y. Carbonization and graphitization of polyimide film "Novax". *Carbon* **1991**, *29*, 1239−1243.
(18) Ramachandran, J.; Lu, M.; Arias-Monje, P. J.; Kirmani, M. H.; Shirolkar, N.; Kumar, S. Towards designing strong porous carbon fibers through gel spinning of polymer blends. *Carbon* **2021**, *173*, 724−735.
(19) Ma, L.; Wang, Y.; Niu, F.; Wang, Y.; Zhuang, G.; Qiu, Y.; Zhang, R.; Ma, Q. Structural evolution and thermal property of carbon films prepared with polyimide and polyacrylonitrile. *Mater. Res. Express* **2018**, *6*, 026408.
(20) Zhang, H.; Jiang, S.; Duan, G.; Li, J.; Liu, K.; Zhou, C.; Hou, H. Heat-resistant polybenzoxazole nanofibers made by electrospinning. *Eur. Polym. J.* **2014**, *50*, 61−68.
(21) Sanders, D. F.; Guo, R.; Smith, Z. P.; Liu, Q.; Stevens, K. A.; McGrath, J. E.; Paul, D. R.; Freeman, B. D. Influence of polyimide precursor synthesis route and ortho-position functional group on thermally rearranged (TR) polymer properties: Conversion and free volume. *Polymer* **2014**, *55*, 1636−1647.
(22) Lim, J.; Kim, M.-C.; Goh, M.; Yeo, H.; Shin, D. G.; Ku, B.-C.; You, N.-H. Synthesis and characterization of polybenzoxazole/graphene oxide composites via in situ polymerization. *Carbon Lett.* **2013**, *14*, 251−254.
(23) Tullos, G. L.; Mathias, L. J. Unexpected thermal conversion of hydroxy-containing polyimides to polybenzoxazoles. *Polymer* **1999**, *40*, 3463−3468.
(24) Xie, J.; Yao, L.; Xu, F.; Li, Y.; Shan, Z.; Hui, D.; Qiu, Y. Fabrication and characterization of three-dimensional PMR polyimide composites reinforced with woven basalt fabric. *Composites, Part B* **2014**, *66*, 268−275.
(25) Nam, K.-H.; Choi, H.; Yeo, H.; You, N.-H.; Ku, B.-C.; Yu, J. Molecular design and property prediction of sterically confined polyimides for thermally stable and transparent materials. *Polymers* **2018**, *10*, 630.
(26) Liaw, D.-J.; Chang, F.-C.; Leung, M.-k.; Chou, M.-Y.; Muellen, K. High thermal stability and rigid rod of novel organosoluble polyimides and polyamides based on bulky and noncoplanar naphthalene−biphenyldiamine. *Macromolecules* **2005**, *38*, 4024−4029.
(27) Chern, Y.-T.; Shiue, H.-C. Low dielectric constants of soluble polyimides based on adamantane. *Macromolecules* **1997**, *30*, 4646−4651.
(28) Duan, G.; Jiang, S.; Chen, S.; Hou, H. Heat and Solvent Resistant Electrospun Polybenzoxazole Nanofibers from Methoxy-Containing Polyaramide. *J. Nanomater.* **2010**, *2010*, 1−5.
(29) Zhang, H.; Wang, W.; Chen, G.; Zhang, A.; Fang, X. Melt-Processable Semicrystalline Polyimides Based on 1,4-Bis(3,4-dicarboxyphenoxy)benzene Dianhydride (HQDPA): Synthesis, Crystallization, and Melting Behavior. *Polymers* **2017**, *9*, 420.
(30) Hsiao, S.-H.; Huang, T.-L. Synthesis and Characterization of New Polyimides Based on 3,6-Bis(4-aminophenoxy)benzonorbornane. *J. Polym. Res.* **2004**, *11*, 9−21.
(31) Niu, Y.; Fang, Q.; Zhang, X.; Zhao, J.; Li, Y. Structural evolution, induced effects and graphitization mechanism of reduced graphene oxide sheets/polyimide composites. *Composites, Part B* **2018**, *134*, 127−132.
(32) Saenko, N. S. The X-ray diffraction study of three-dimensional disordered network of nanographites: Experiment and theory. *Phys. Procedia* **2012**, *23*, 102−105.
(33) Weng, M.; Jian, L.; Feng, X.; Luo, X.; Hu, J.; Zhang, J.; Liu, Y.; Min, Y. High oriented graphite film with high thermal conductivity prepared by pure polyimide film formed with catalyst pyridine. *Ceram. Int.* **2021**, *47*, 24519−24526.
(34) Ma, L.; Wang, Y.; Wang, Y.; Wang, C.; Gao, X. Graphene induced carbonization of polyimide films to prepared flexible carbon films with improving-thermal conductivity. *Ceram. Int.* **2020**, *46*, 3332−3338.
(35) Xiao, M.; Zhang, X.; Xiao, W.; Du, J.; Song, H.; Ma, Z. The influence of chemical constitution on the structure and properties of polyimide fibre and their graphite fibre. *Polymer* **2019**, *165*, 142−151.
(36) Tao, Z.; Wang, H.; Lian, P.; Zhang, J.; Liu, Z.; Guo, Q.; Liu, L. "Graphitic bubbles" derived from polyimide film. *Carbon* **2017**, *116*, 733−736.

https://doi.org/10.1021/acsomega.2c02731
ACS Omega 2022, 7, 25565−25572